JACS Au
AN OPEN ACCESS JOURNAL OF THE AMERICAN CHEMICAL SOCIETY

pubs.acs.org/jacsau

Article

Strong, Multifaceted Guanidinium-Based Adhesion of Bioorganic Nanoparticles to Wet Biological Tissue

Lam Tan Hao,[○] Sohee Park,[○] Seunghwan Choy,[○] Young-Min Kim, Seung-Woo Lee, Yong Sik Ok, Jun Mo Koo, Sung Yeon Hwang,* Dong Soo Hwang,* Jeyoung Park,* and Dongyeop X. Oh*

Cite This: *JACS Au* 2021, 1, 1399–1411

Read Online

ACCESS | Metrics & More | Article Recommendations | Supporting Information

ABSTRACT: Gluing dynamic, wet biological tissue is important in injury treatment yet difficult to achieve. Polymeric adhesives are inconvenient to handle due to rapid cross-linking and can raise biocompatibility concerns. Inorganic nanoparticles adhere weakly to wet surfaces. Herein, an aqueous suspension of guanidinium-functionalized chitin nanoparticles as a biomedical adhesive with biocompatible, hemostatic, and antibacterial properties is developed. It glues porcine skin up to 3000-fold more strongly (30 kPa) than inorganic nanoparticles at the same concentration and adheres at neutral pH, which is unachievable with mussel-inspired adhesives alone. The glue exhibits an instant adhesion (2 min) to fully wet surfaces, and the glued assembly endures one-week underwater immersion. The suspension is lowly viscous and stable, hence sprayable and convenient to store. A nanomechanic study reveals that guanidinium moieties are chaotropic, creating strong, multifaceted noncovalent bonds with proteins: salt bridges comprising ionic attraction and bidentate hydrogen bonding with acidic moieties, cation−π interactions with aromatic moieties, and hydrophobic interactions. The adhesion mechanism provides a blueprint for advanced tissue adhesives.

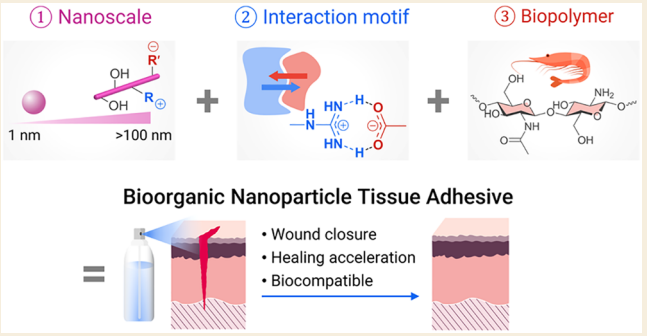

KEYWORDS: *bioorganic nanoparticles, tissue adhesive, guanidinium, surface chemistry, noncovalent interactions, chitin, hemostasis, antibacterial properties*

INTRODUCTION

In injury treatment and surgery, wound closure is required to bind wet-tissue incisions and prevent fluid leakage.[1,2] To boost tissue regeneration, polymeric adhesives are replacing sutures and staples, which are invasive and not applicable to inaccessible body parts.[2]

Developing polymeric adhesives for soft, wet tissue is challenging because swelling, particularly of hydrophilic polymers, alters mechanical properties of adhesives, leading to cohesion failure, poor tissue adhesion, and detrimental tissue compression.[1,3] Polymeric adhesives are also too viscous to handle after cross-linking reactions cascade, resulting in poor contact with dynamic tissue,[4] and they are difficult to spray or apply evenly on substrates.

Most clinically available adhesives do not satisfy performance and biocompatibility requirements. Most petrochemical adhesives and some biobased adhesives are cytotoxic and often accompany heat, pH change, and/or chemical reaction when curing which can traumatize patients.[2] For example, mussel-inspired adhesives require alkaline conditions or cytotoxic mediators such as ferric (Fe^{3+}) or periodate (IO_4^-) for cross-linking.[1,5] They also need to be stored and distributed under reduced oxygen conditions before *in vivo* application because their autoxidation results in gradual loss of adhesion strength and generation of tissue-damaging reactive oxygen species upon exposure to air.[1,3,5,6] While natural adhesives are more biocompatible, they usually weakly adhere under physiological conditions.[1,2]

The design of next-generation tissue adhesives requires one to integrate high performance, convenience, and biocompatibility into one material. Aqueous inorganic nanoparticle suspensions are simple and efficient glues for gluing hydrogels and tissue through physical bridging without chemical cross-linkers.[7−15] Although they are convenient to handle and store because of oxidation resistance and low viscosity, the health risks associated with inorganic nanoparticles remain concerning.[16] Moreover, they weakly adhere to tissue because the adhesion relies on the van der Waals interaction.[17]

Surface modification can improve nanoparticle adhesion. In this regard, interactions mediated by the guanidinium cation (Gua^+) in biological systems are a great inspiration. Gua^+ is

Received: May 4, 2021
Published: September 8, 2021

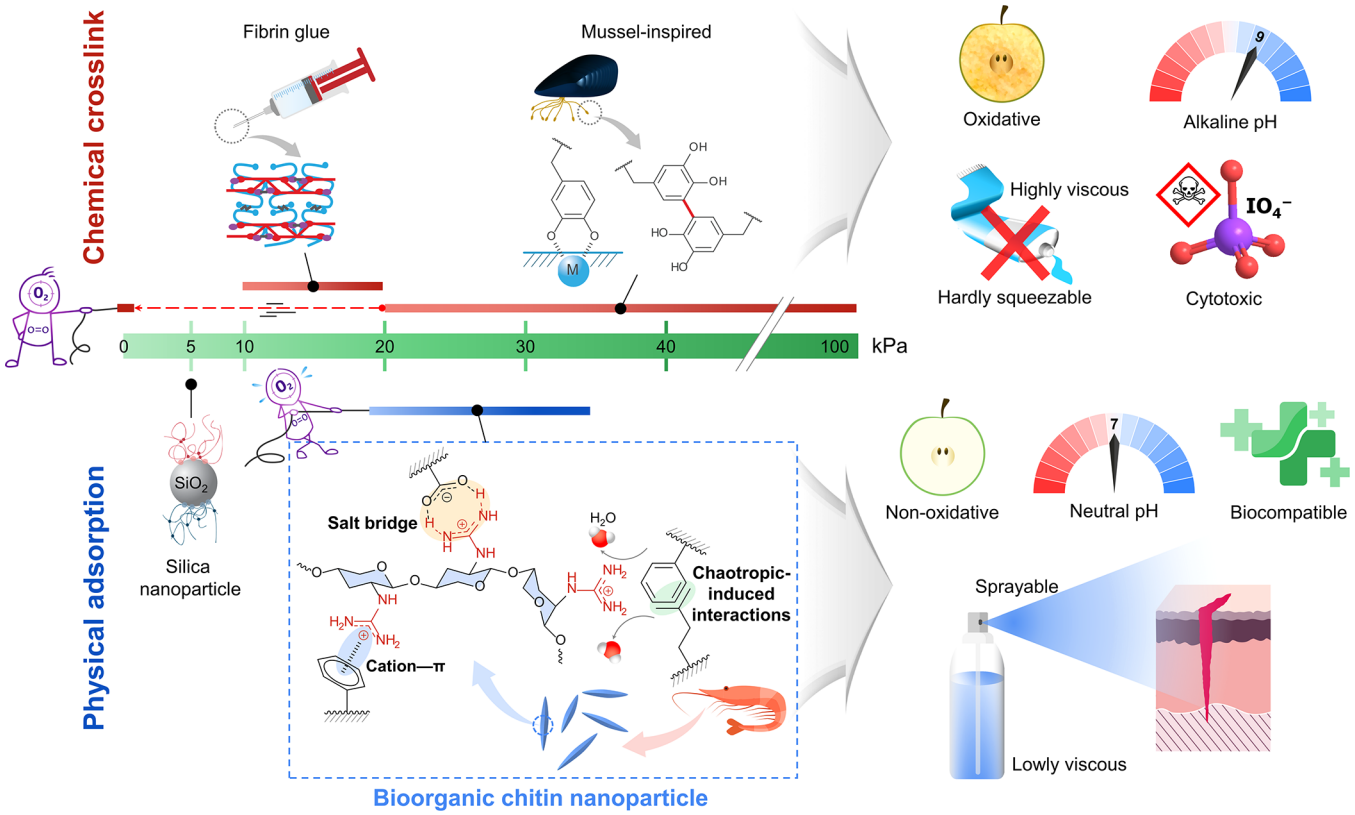

Figure 1. Schematic illustration of various tissue adhesives and their adhesion strength ranges. Compared with physical adsorption-based nanoparticle suspension adhesives, the performance, storage, and handling of chemically cross-linked adhesives are limited by spontaneous oxidation, high viscosity, and nonbiocompatible cross-linking conditions. The adhesion mechanism of the bioorganic chitin nanoparticle through guanidinium-mediated multifaceted noncovalent interactions is proposed.

found mainly in the side chain of arginine (Arg) that modulates adhesion of biomolecules.[18] Gua^+ forms strong, multifaceted noncovalent interactions under aqueous conditions, including bidentate hydrogen-bond-associated salt bridges with oxyanions, and cation−π interactions with aromatic moieties;[18] Gua^+ can also manifest hydrophobic interactions.[19] These properties stem from its planar structure that sterically hinders water molecules and dehydrates the Gua^+ surface (chaotropic effect).[20] Moreover, owing to its high pK_a (>12.5), Gua^+ remains fully protonated at physiological pH, which is necessary for binding.[21] These unique features of Gua^+, however, have not been recognized for the fabrication of wet tissue adhesives.

Achieving excellent adhesion also requires a high cohesion energy of the adhesive to effectively dissipate energy.[1,4] In this respect, bioorganic chitin and chitosan, its deacetylated derivative, satisfy this requirement owing to their highly crystalline structures resulting from collective intermolecular hydrogen bonding.[1] They also exhibit biological functions (e.g., hemostatic and antibacterial properties)[22] that accelerate wound healing. Chemically modified chitin and chitosan have been used as hydrogel tissue adhesives,[23,24] which suffer disadvantages of excess swelling and difficult handling mentioned above. As nanomaterials, they were used as reinforcing fillers for polymeric adhesives without directly exhibiting adhesive properties (Figure S1a).[23,25] The use of chitin nanoparticles as adhesives for dry, hard surfaces through long-range, self-assembled structure has also been reported.[26] However, in this system water evaporation is required to induce the self-assembly of chitin nanoparticles, and the adhesion is completely lost upon rehydration,[26] thus not applicable to wet, dynamic surfaces like biological tissue (Figure S1b).

Herein, we fabricate a glue for soft, wet substrates containing an aqueous suspension of *N*-guanidinium chitosan nanowhiskers (G-CSW), combining the beneficial features of nanoparticle suspensions, Gua^+-mediated interactions, and chitosan (Figure 1; Movie S1). The glue greatly adhered to porcine skin (30 kPa), 2-fold more strongly than fibrin glue, and up to 3000-fold stronger than inorganic nanoparticles when normalized by concentration. G-CSW instantly adhered to fully wet surfaces, resisted hydration-induced dissolution, and worked at physiological pH. It is easy to spray on adherends (Movie S2) and does not require stringent storage conditions. We also elucidated the roles of multifaceted noncovalent Gua^+-mediated interactions in the adhesion mechanism. The inherent biological benefits of G-CSW provide additional advantages for tissue regeneration.

RESULTS AND DISCUSSION

Designing and Characterizing Bioorganic Nanoparticle Adhesives

The mechanism of gluing soft, wet substrates with nanoparticles is that polymer chains of the substrate are physically adsorbed onto the surface of nanoparticles, which act as connectors between polymer chains (Figure S1c).[7] Adsorption density and strength depend on the type and number of interfacial substrate−nanoparticle noncovalent bonds. Generally, inorganic−organic interfacial interactions are weaker

https://doi.org/10.1021/jacsau.1c00193
JACS Au 2021, 1, 1399−1411

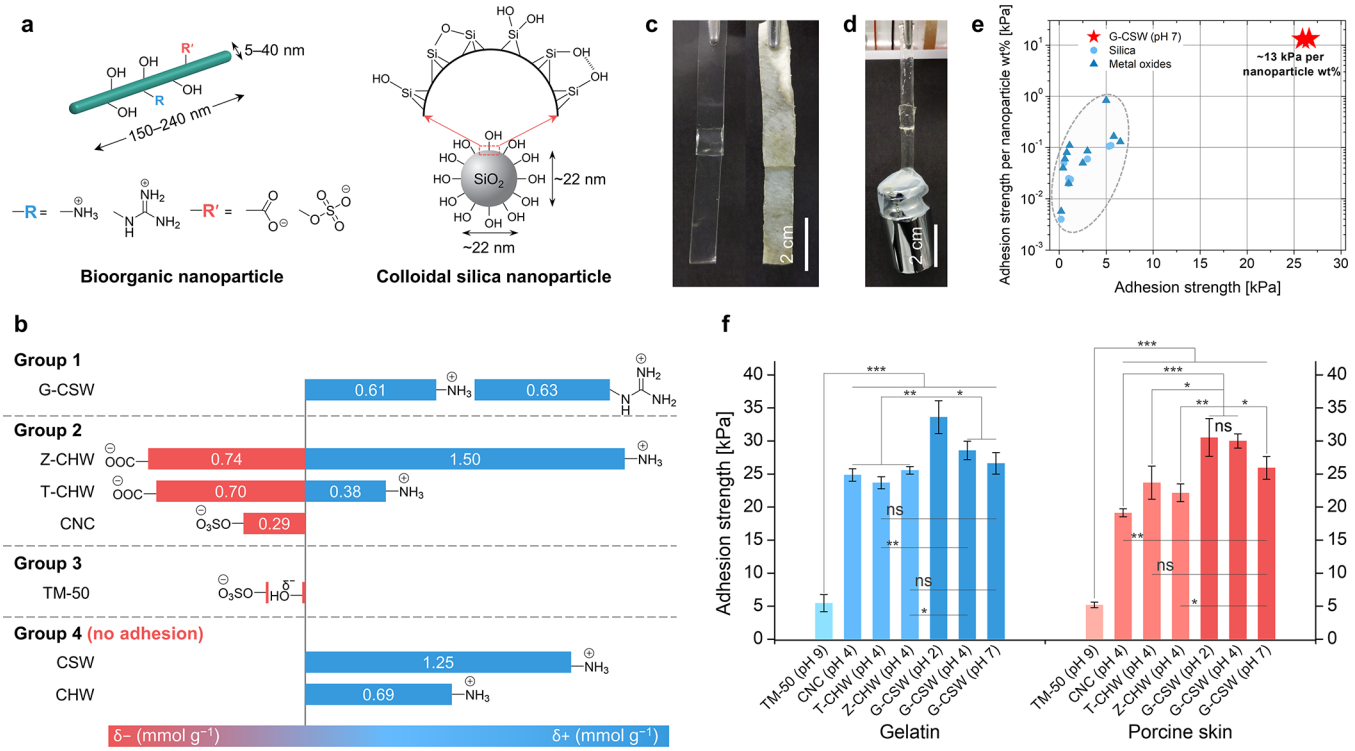

Figure 2. Characterization and adhesion of nanoparticles to soft, wet substrates. (a) Dimensions and surface chemistry of bioorganic and TM-50 silica nanoparticles. (b) Classifying nanoparticles based on their adhesion abilities and surface groups (R and R′). (c) Representative photographs showing the gluing of two pieces of (left) gelatin hydrogel and (right) porcine skin using 30 μL of aqueous G-CSW suspension (2 wt %, pH 7) over 100 mm^2 substrate surface. (d) A gelatin assembly with 100 mm^2 adhesion area withstands a 200 g weight (Movie S1). (e) Ashby plot of adhesion strengths normalized by concentration of bioorganic G-CSW in this study and inorganic nanoparticles from literatures (Table S5). (f) Adhesion strengths under normal conditions on gelatin hydrogels (23 wt %) and porcine skin glued with various 2 wt % nanoparticle suspensions, measured after curing the assemblies for 1 h. Only G-CSW showed adhesion at pH 7. The data are expressed as means ± standard deviations of triplicate. Student's t test was used for comparison (*p < 0.05; **p < 0.01; ***p < 0.001; ns, no significance).

than organic−organic counterparts. Therefore, bioorganic nanoparticles with surface functionality interacting strongly and multivalently with the substrate are desirable.

Chitin, one of the most abundant biopolymers, can be transformed into one-dimensional (1D) nanoparticles.[27,28] Moreover, chitin is readily modifiable owing to the amino group in its repeating unit. The resulting nanoparticles can combine the surface-modified adhesion property with the biological advantages of the biopolymer. They are dispersible but insoluble in water owing to their highly crystalline structures.[1]

In addition to G-CSW, four types of chitin nanoparticle were prepared:[28] chitin nanowhiskers (CHW), chitosan nanowhiskers (CSW), 2,2,6,6-tetramethylpiperidine-1-oxyl (TEMPO)-mediated oxidized CHW (T-CHW), and zwitterionic CHW (Z-CHW) (Scheme S1). Commercial cellulose nanocrystals (CNC) and silica nanoparticles (TM-50) were included for comparison. Material information is summarized in Figure 2a,b and Table S1. While the spherical silica material is 22 nm in diameter, the other 1D bioorganic nanoparticles are approximately 150−240 nm long and 5−40 nm wide (Figures S2 and S3). The bioorganic nanoparticles have hydroxy groups on their surfaces and are distinguishable by their functional groups (cationic R and anionic R′).

CHW was prepared by β-(1→4)-glycosidic hydrolysis of the amorphous region of bulk chitin; it has an amino content of 0.69 mmol g^{-1}; surface deacetylation of CHW afforded CSW with a nearly 2-fold higher amino density (1.25 mmol g^{-1}). The surface C6-hydroxy groups of chitin and partially deacetylated chitin were oxidized by TEMPO to give T-CHW and Z-CHW, respectively, with carboxylate contents of 0.70−0.74 mmol g^{-1}. Z-CHW has an amino content four times that of T-CHW (1.5 vs 0.38 mmol g^{-1}). CHW has a higher amino content than T-CHW, which is attributable to partial acidic hydrolysis of acetamide moieties. G-CSW was obtained by scandium(III) triflate-catalyzed guanylation of CSW,[29] (Scheme S1; Figure S4) wherein ∼50% of the amino groups were converted into guanidinium groups (0.63 mmol g^{-1}). CNC produced by sulfuric acid (H_2SO_4)-hydrolysis of pulp[30] has a sulfate-half-ester (OSO_3^-) concentration of 0.29 mmol g^{-1}, while TM-50 only contains siloxane (Si−O−Si) and silanol (Si−OH) functionalities with a trace amount of sulfate (Figure 2b; Figures S5 and S6; Table S2).

Nanoparticle Adhesion to Soft, Wet Substrates

We prepared 1-, 2-, and 3-wt % aqueous bioorganic nanoparticle suspensions at pH 4 and 7 by sonication. Particle aggregation was prevented by adjusting the suspension pH with a few drops of HCl/NaOH to maintain a low ionic strength.[30] These suspensions were much less viscous (9.14−13.3 cP at 3 wt %) than polymeric gel adhesives (Table S3), hence sprayable on substrates (Movie S2). The inorganic TM-50 suspension (50 wt %, pH ∼ 9)[7] is stable under alkaline conditions as neutralization results in gelation due to acid-catalyzed reactions of the SiOH groups.[31]

The adhesion performance of the nanoparticle suspensions was evaluated on porcine skin-derived gelatin hydrogels (23 wt

https://doi.org/10.1021/jacsau.1c00193
JACS Au 2021, 1, 1399−1411

%) and porcine skin. General adhesion performance is discussed in terms of the substrate and the concentration and pH of the nanoparticle suspension. Both substrates are chemically similar, thus yielded similar results with the suspensions. Their amino acid profiles are abundant in nonpolar (~73 mol %) and hydroxylated (6−6.9 mol %) residues. Both substrates contain substantial amounts of negatively and positively charged residues (11.9−12.9 and 8.1−8.7 mol %, respectively). Gua^+-bearing arginine accounts for >50% of positively charged amino acids (Figure S7; Table S4). While the 1 wt % suspensions did not glue the substrates, the 2 and 3 wt % suspensions exhibited similar adhesion performance (Figure 2c−f; Figure S8). We speculate that the accessible surface area of the substrates is mostly saturated when >2 wt % bioorganic nanoparticle suspensions are applied. Among the bioorganic nanoparticles, only G-CSW suspensions could glue under neutral conditions, which is an advantage for biomedical applications over mussel-inspired adhesives requiring alkaline conditions for oxidative cross-linking.[1]

Depending on maximum adhesion strength (after curing the assemblies for 1 h), the nanoparticles can be classified into four groups (Figure 2b,f). Group 1 including Gua^+-bearing G-CSW adhered the strongest to the substrates (26−33 kPa), 1.5−2-times stronger than fibrin glue,[1] and overlaps the range of some mussel-inspired adhesives[6,32] (Figure 1). Group 2 (T-CHW, Z-CHW, and CNC) adhered with intermediate strengths (19−25.5 kPa); their surfaces bear negatively charged functional groups (COO^- or OSO_3^-). Group 3 contains TM-50, which bears SiOH but no ionic functional groups; it adhered significantly more weakly (5−5.5 kPa). Group 4 (CHW and CSW) did not adhere; they bear varying amounts of NH_3^+ on their surfaces. Most noticeably, the adhesion strength capacity normalized by nanoparticle concentration of G-CSW is one to three orders of magnitude greater than previous studied inorganic nanoparticles (Figure 2e; Table S5).[7−15] This implies that the use of bioorganic nanoparticles can help overcome the synthetic challenge of inorganic nanoparticle manufacturing.

In addition, study on the instant adhesion ability of Group 1−3 nanoparticles revealed that bioorganic nanoparticles (Group 1 and 2) reached ~50% of their maximum adhesion strength after only 2 min curing, in contrast to inorganic nanoparticles (Group 3), which required at least 15 min of curing to exhibit adhesion. The adhesion strength increased with time because more nanoparticles absorb and bridge two substrate surfaces. After 15 min of curing, the adhesion performance of all nanoparticles was essentially similar to that after 60 min of curing (Figure S9). These results showcase the compatibility of organic−organic over inorganic−organic interfacial interactions.

The different adhesion behavior of these groups is attributed to aqueous dispersibility, surface functional groups, and interparticle cohesion. First, a stable nanoparticle dispersion provides large interfacial area for effective adsorption of substrate polymers. By contrast, aggregated particles lead to a macroscopic barrier between the adhered surfaces.[7,8] The pK_a of Gua^+ is >12.5;[21] NH_3^+, ~6.5;[33] COOH, ~3.6;[34] and OSO_3H, 2.5.[35] All nanoparticles are well-dispersed at pH 4 due to cationic repulsion between Gua^+ (G-CSW) or NH_3^+ (CHW, CSW, Z-CHW, and T-CHW), and anionic repulsion between the OSO_3^- of CNC. The colloidal stability of the acidic suspensions was confirmed by their high zeta potential (absolute) values (Figure S10). Among the positively charged nanoparticles, only G-CSW remained well-dispersed over a prolonged period at pH 7 (Figure S4d); the high pK_a of Gua^+ leads to a high zeta potential of +27.9 mV. Consequently, only G-CSW glued gelatin hydrogels and porcine skin at neutral pH. However, despite being dispersed at pH 7, neither CNC nor T-CHW adhered well. While the COOH groups of the substrate acidic residues are partially deprotonated at pH 4, they are fully deprotonated at pH 7 and are more strongly repelled by the negatively charged nanoparticles.

Surface functional groups comprise the second factor. Adhesion is the result of the net energy associated with substrate−nanoparticle interfacial noncovalent interactions. Attractive interactions, including hydrogen bonding, salt bridging, π-associated, and van der Waals interactions, counteract repulsive forces between similar charges. Attractive interactions can be screened by ion hydration. For example, compared with the NH_3^+/COO^- pair, the interaction energy of the Gua^+/COO^- pair is weaker in gas but stronger in water because Gua^+ is less hydrated than NH_3^+,[18,20] as reflected in the extreme adhesion difference exhibited by Groups 1 and 4. Furthermore, linear correlation analyses revealed that the adhesion of chitin nanoparticles to gelatin hydrogels was stronger with increasing Gua^+ concentration (Pearson's correlation coefficient, $R > 0.9$) but unaffected by NH_3^+ concentration ($R = -0.565$) (Figure S11). Group-2 adhesion is attributable to COO^-- or OSO_3^--mediated adsorptions of nanoparticles onto Gua^+-bearing Arg residues in the proteinaceous substrate. Because of the lower Arg abundance compared with the negatively charged residues of the substrate, Group 2 adhered more weakly than Group 1. TM-50 (Group 3) contains no charged groups; hence, only van der Waals interactions on nanospheres can bridge substrate polymer chains.[17] These observations prompt us to investigate the Gua^+-mediated adhesion mechanism.

The effect of dispersibility and surface functional group on the adhesion of nanoparticles can be confirmed by lowering the suspension pH to 2. Under this condition, anionic Group 2 nanoparticles (except Z-CHW) aggregated with a zeta potential (absolute value) of <20 mV (Figures S10 and S12) due to the protonation of anionic groups. Thus, CNC and T-CHW lost their adhesion ability. Z-CHW was well dispersible because of its abundant surface NH_3^+ groups, but the nanoparticle could not glue gelatin and porcine skin because NH_3^+ groups are extensively hydrated, which is similar to Group 4 nanoparticles. G-CSW was well dispersible and exhibited an elevated adhesion strength of >30 kPa on proteinaceous substrates due to a greater protonation degree and the chaotropicity of Gua^+ moieties (Figure 2f).

The third factor is a high cohesion energy of organic nanoparticles resulting from collective intermolecular hydrogen bonding, which leads to a 6-fold improvement in adhesion strength when transitioning from inorganic to organic nanoparticles.[1,33] Indeed, once lyophilized, the redispersion of bioorganic nanoparticles in water requires high-energy sonication to break interparticle hydrogen bonds.

Macroscopic and Molecular-Level Adhesion Mechanism

We studied the adhesion mechanism of the bioorganic nanoparticles at the macroscopic level by dividing the constituent side chains of the proteinaceous substrates into neutral, polar, anionic, and cationic components. To that end, we prepared hydrogels different in the functional group and electrical charge on their side chains, including neutral, polar

https://doi.org/10.1021/jacsau.1c00193
JACS Au 2021, 1, 1399−1411

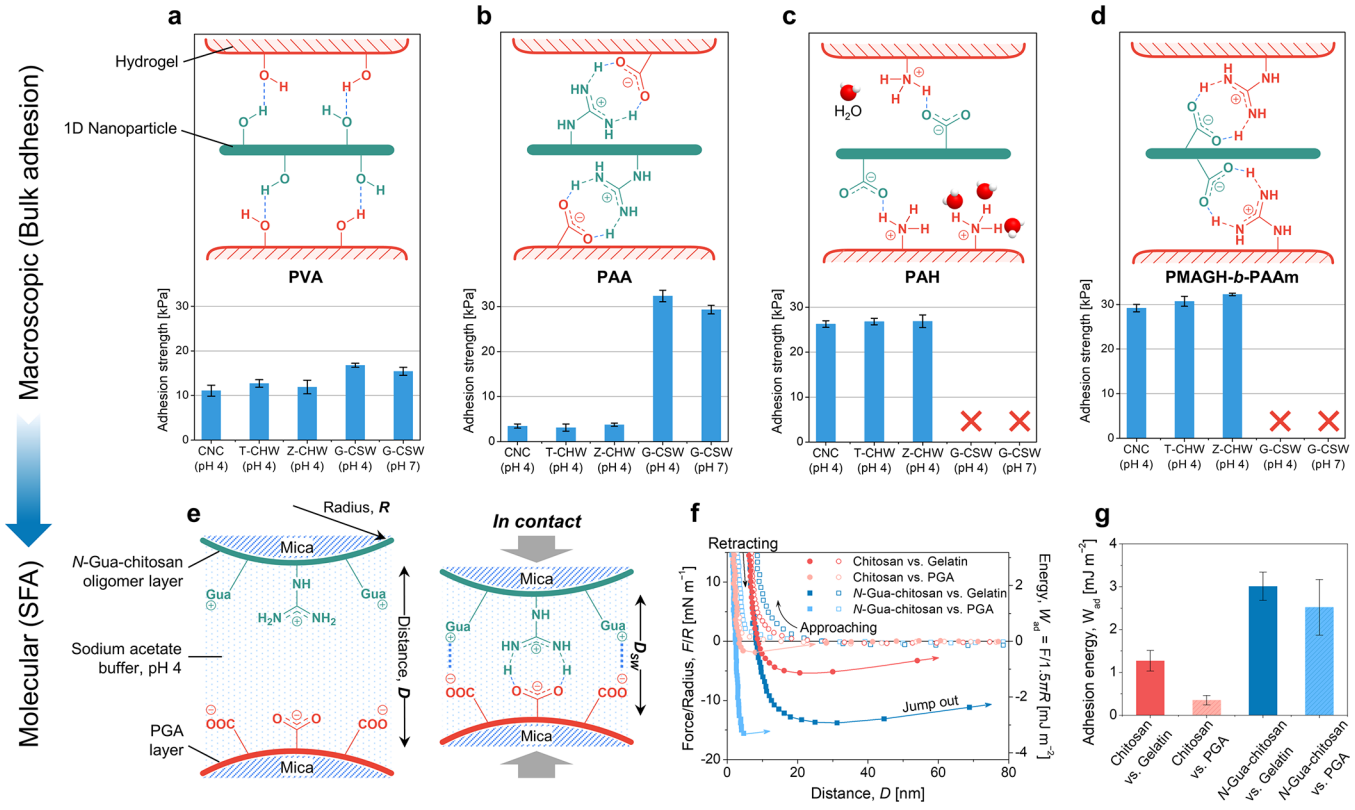

Figure 3. Adhesion mechanics of bioorganic nanoparticles at the macroscopic and molecular levels. (a–d) Bulk adhesion tests: (top) major interactions responsible for adhesion between functional groups of the nanoparticle and the substrate, and (bottom) adhesion strength of 2 wt % bioorganic nanoparticle suspensions on various hydrogels. (a) PVA, (b) PAA, (c) PAH, and (d) PMAGH-*b*-PAAm. X's indicate no adhesion. The adhesion strength data are expressed as means ± standard deviation of triplicates. (e–g) SFA data. (e) Schematic representation of measuring the surface adhesion showing salt bridge interactions between mica surfaces coated with poly(glutamic acid) (PGA) and *N*-guanidinium chitosan oligosaccharide. (f) Representative force–distance profiles and (g) corresponding interaction energies between two differently coated mica surfaces in 10 mM sodium acetate buffer at pH 4. Chitosan and PGA were used as control layers. The SFA data are expressed as means ± standard deviations of quadruplicates.

poly(vinyl alcohol) (PVA), anionic polyacrylate (PAA), cationic poly(allylamine hydrochloride) (PAH), and cationic poly(methacryl guanidine hydrochloride)-*block*-polyacrylamide (PMAGH-*b*-PAAm) (Scheme S2; Figures S13 and S14). The relationships between individual substrate–nanoparticle functional-group interactions and adhesive strength were independently determined by examining the abilities of 2 wt % suspensions of Group 1 and 2 nanoparticles to adhere to the four hydrogels (Figure 3a–d; Figure S15).

All nanoparticles adhered with similar strengths to PVA (11.1–16.8 kPa) but less strongly to gelatin and porcine skin. In this system, hydrogen bonding between hydroxy groups governs the polymer chain adhesion to the nanoparticle surface (Figure 3a). Adhesion of nanoparticles to PAA is considerably different; the negatively charged nanoparticles are repelled by the COO^- of PAA, resulting in inefficient adhesion. In contrast, G-CSW adhered more strongly (~33 kPa) because Gua^+ forms a multivalent salt bridge with COO^- (Figure 3b).[18] Opposite trends were observed for the cationic hydrogels; G-CSW did not adhere due to strong repulsion between nanoparticle Gua^+ groups and substrate cationic groups. However, negatively charged nanoparticles efficiently glued the substrates. Adhesion to the Gua^+-based hydrogel was stronger (up to 32.3 kPa) than the primary amino-based hydrogel (26.9 kPa) due to the chaotropic nature of Gua^+ (Figure 3c,d).

The nanomechanics of Gua^+ and NH_3^+ moieties were compared at the molecular level at pH 4 using a surface forces apparatus (SFA). Chitosan and *N*-guanidinium chitosan (*N*-Gua-chitosan) oligosaccharides were used to effectively coat mica surfaces and avoid roughness caused by nanoparticles. The opposite mica surface was coated with gelatin or poly(glutamic acid) (PGA; pK_a of side chain COOH, 2.16). The adhesion forces were recorded as a function of the mica–mica distance (D). The surfaces were brought into contact at the steric wall distance (D_{sw}), where the distance between the two surfaces does not significantly change with increasing compressive force (Figure 3e). An adhesion force (F_{ad}/R) of 14 mN m^{-1}, corresponding to an adhesion energy (W_{ad}) of 3.0 mJ m^{-2}, was recorded for the *N*-Gua-chitosan/gelatin surfaces after 10 min contact; these values are 2.3-times higher than those of the chitosan/gelatin surfaces (6 mN m^{-1} and 1.3 mJ m^{-2}). W_{ad} values for the NH_3^+/COO^- and Gua^+/COO^- salt bridges were determined to be 0.35 and 2.5 mJ m^{-2}, respectively, from interactions between the corresponding oligosaccharides and PGA (Figure 3f,g). Using association constants of 0.31 and 0.37 M^{-1} (ref 18), binding energies of 2.903 and 2.464 kJ mol^{-1} were calculated for the NH_3^+/COO^- and Gua^+/COO^- salt bridges, respectively (Figure S16). Calculation of salt bridge interaction efficiency underwater revealed one salt bridge per 13.8 nm^2 for NH_3^+/COO^- and per 1.64 nm^2 for Gua^+/COO^- (Supporting Information). Thus,

https://doi.org/10.1021/jacsau.1c00193
JACS Au 2021, 1, 1399–1411

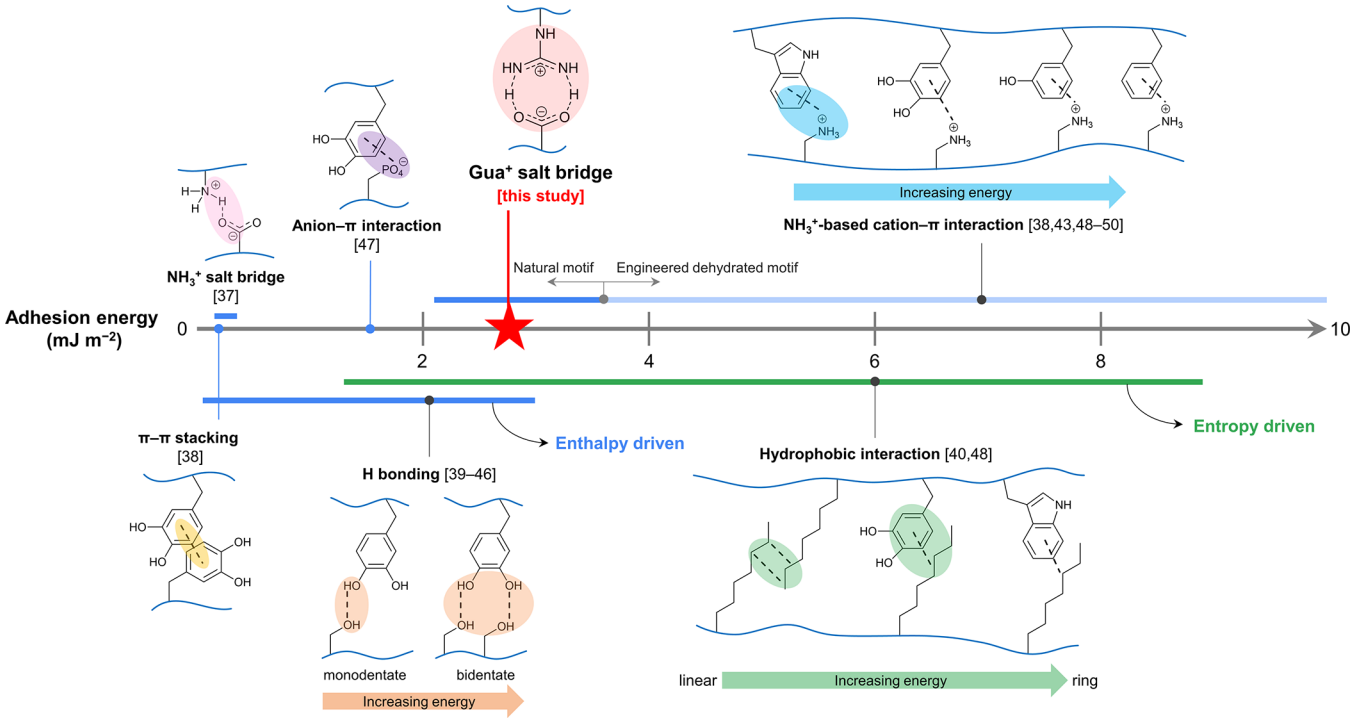

Figure 4. Comparing noncovalent interactions underwater. Linear scale of underwater adhesion energies per unit area in mJ m^{-2}. The energy of the guanidinium-mediated salt bridge in this study is shown along with those of other motifs reported in the literature obtained under aqueous conditions using a surface forces apparatus (Table S6). Reference numbers are shown in brackets. Blue scales represent enthalpy-driven forces (electrostatic attraction), and the green scale represents stronger entropy-driven processes (dehydration effect). The Gua^+ salt bridge exhibits both characteristics.

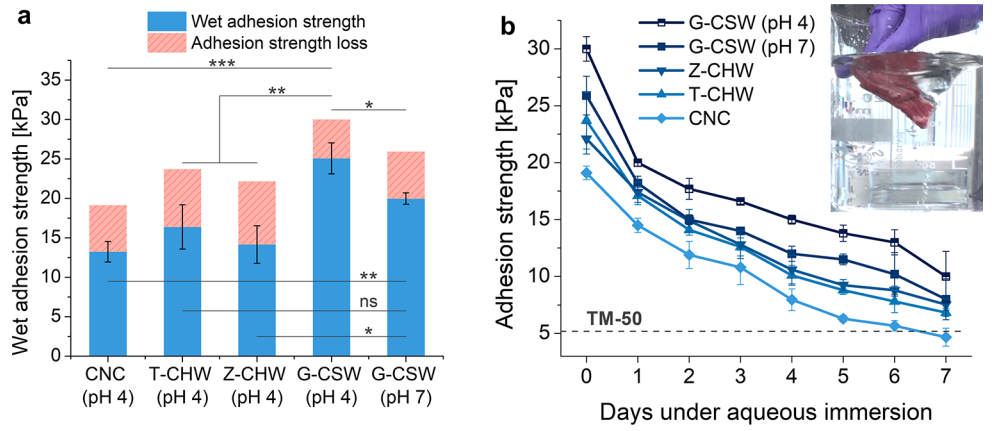

Figure 5. (a) Adhesion strengths of bioorganic nanoparticle suspensions (2 wt %) on fully wetted porcine skin measured at 1 h after nanoparticle application. The data are expressed as means ± standard deviations of triplicates. Student's *t* test was used for comparison (*$p < 0.05$; **$p < 0.01$; ***$p < 0.001$; ns, no significance). Adhesion strength loss due to surface wetting is the difference between adhesion strength on porcine skin at its natural state (Figure 2f) and that on wetted porcine skin. (b) Underwater resistance of adhered porcine skin assembly using bioorganic nanoparticle suspensions (2 wt %) after curing for 1 h with the skin assemblies immersed in phosphate buffered saline (pH 7.4) for 1 week. Data are expressed as means ± standard deviations of triplicates. Inset: a beef assembly glued with the G-CSW suspension (2 wt %, pH 7) sustained strong stirring underwater. Failure occurred at 22.5 s with increasing stirring rate. The frame was captured from Movie S3.

Gua^+ is 8.4-times more effective than NH_3^+ in forming interactions in the aqueous solution.

Because negatively charged residues constitute 12 mol % of gelatin and the two bare gelatin surfaces do not adhere to each other, other types of interaction are involved in adhering G-CSW to gelatin. The Gua^+ moiety can form cation–π interactions with Phe, His, or Tyr residues, and chaotropicity can lead to hydrophobic interactions between nonpolar residues of the two gelatin surfaces (Figure 1).[18,19]

Next, we compared the adhesion energy of the Gua^+/COO^- salt bridge in this study with literature data for noncovalent interactions in aqueous environments. SFA-measured interaction energies are detailed in Table S6 and plotted in Figure 4. The Gua^+-mediated salt bridge (2.5–5.6 mJ m^{-2})[36] is among the strongest noncovalent bond, outperforming general salt bridges (0.15–0.35 mJ m^{-2}),[37] π–π stacking (0.2 mJ m^{-2}),[38] hydrogen bonding (0.05–2.99 mJ m^{-2}),[39−46] anion–π interactions (1.54 mJ m^{-2}),[47] and naturally occurring cation–π

https://doi.org/10.1021/jacsau.1c00193
JACS Au 2021, 1, 1399–1411

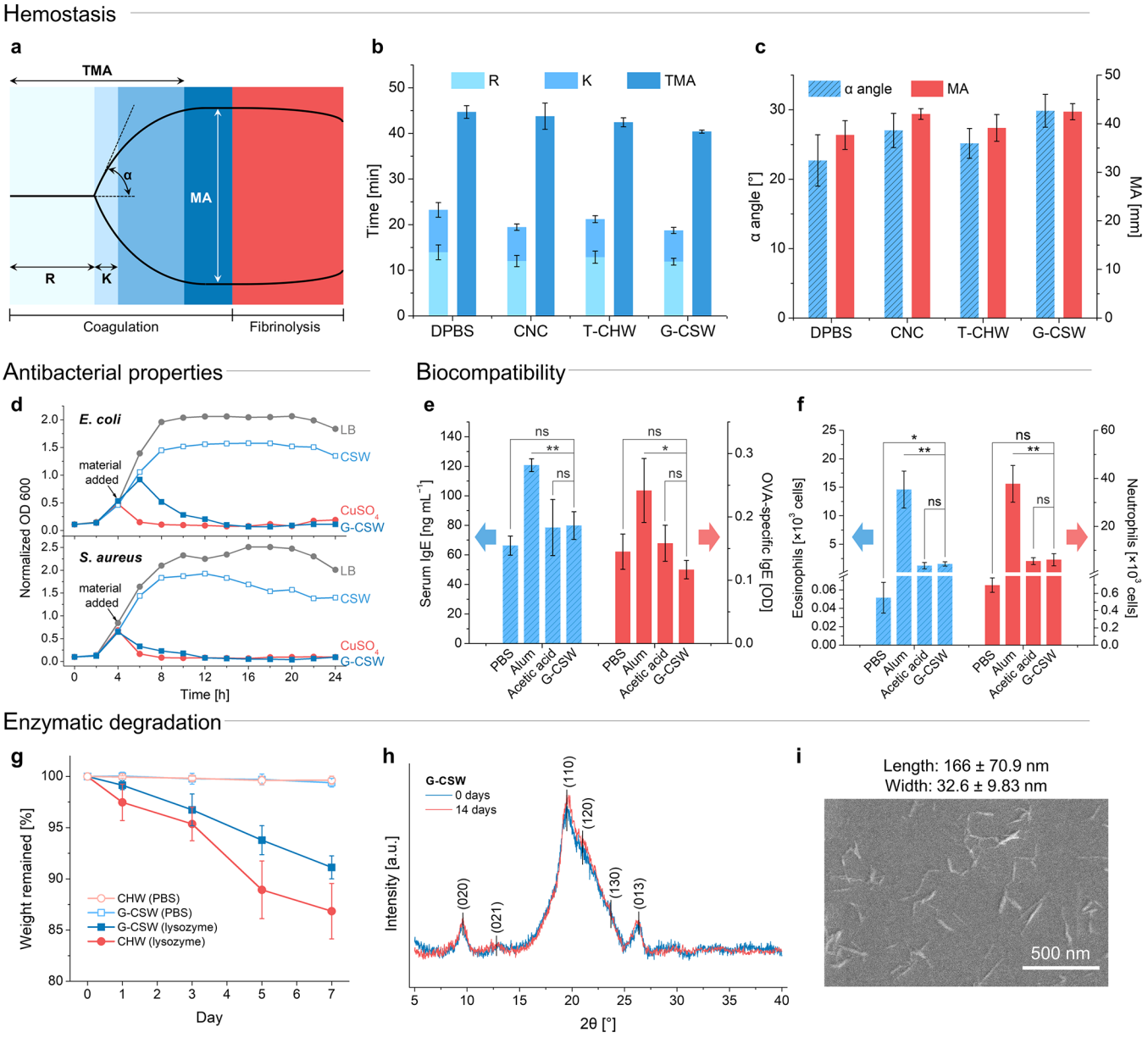

Figure 6. Biological properties of nanoparticle adhesives. (a–c) Hemostatic dynamics using dog blood. (a) Thromboelastogram (TEG) demonstrating the development of blood clots and clot strength over time and corresponding parameters: (b) *R* is the time from the start of testing to clot formation, *K* is the time taken for the blood clot to reach a certain strength, and TMA is the time for the blood clot to reach maximum strength; (c) α angle is the rate of fibrin accumulation, and MA is the maximum strength of the blood clot. Materials were used as 2 wt % suspensions, and Dulbecco's phosphate buffered saline (DPBS) was used as a negative control. (d) Antibacterial activities against Gram-negative *Escherichia coli* and Gram-positive *Staphylococcus aureus* obtained by monitoring bacterial growth curves in lysogeny broth at 37 °C containing various materials. Nanoparticles were used at 0.2 wt %, lysogeny broth was regarded as the negative control, and 0.1 M $CuSO_4$ solution was used as the positive control. (e,f) *In vivo* biocompatibility testing of G-CSW in a mouse model of asthma induced by ovalbumin (OVA). (e) Total and OVA-specific IgE levels in serums. (f) Eosinophil and neutrophil counts in bronchoalveolar lavage fluids. Controls are PBS, blank; acetic acid, negative; and alum (aluminum hydroxide) adjuvant, positive. (g–i) *In vitro* degradation of G-CSW using lysozyme at 37 °C. (g) Weight change after one-week incubation, PBS (0.1 M, pH 7.4) without lysozyme was used as a negative control. (h) XRD patterns G-CSW before (0 days) and after (7 days) treatment with the enzyme. Major crystallographic planes of α-chitin are shown (Figure S24). (i) SEM image showing the preserved needle-like morphology and dimension (average of 100 nanowhiskers) of G-CSW after 1 week of incubation in the enzyme. Data are expressed as means ± standard deviations of triplicates. Student's *t* test was used for comparison (*p < 0.05; **p < 0.01; ***p < 0.001; ns, no significance).

interactions (up to 3.6 mJ m^{-2}).[44,48] Energies of 10 mJ m^{-2} for NH_3^+-mediated cation–π interactions have only been reported under artificially designed dehydrated conditions.[38,43,48−50] Moreover, Gua^+-mediated cation–π interactions are expected to be stronger than those involving NH_3^+. The formation of the Gua^+ salt bridge is driven both enthalpically and entropically by chaotropicity and thus share the energy range with strong entropically driven hydrophobic interactions.[40,48] These results elucidate the substrate–nanoparticle interfacial interactions and highlight the potential of incorporating Gua^+-mediated noncovalent interactions for improving underwater adhesion.

https://doi.org/10.1021/jacsau.1c00193
JACS Au 2021, 1, 1399−1411

Underwater Adhesion

To demonstrate the applicability of nanoparticle adhesives under aqueous conditions in the human body, we examined their adhesion on fully wetted porcine skin. The skin was wetted by immersing in deionized water to which nanoparticle suspensions were directly applied without surface drying. Adhesion strengths on the wetted assembly were measured at 1 h after nanoparticle application. All bioorganic nanoparticles showed decreased adhesion strengths (G-CSW by 17−25%; anionic nanoparticles by >30%) (Figure 5a) because water creates a barrier that dilutes the suspensions and prevents effective adsorption of nanoparticles to the substrate. To simultaneously investigate instant and wet adhesion, we measured the adhesion strengths to wetted porcine skin at 2 min after nanoparticle application. Only G-CSW could instantly absorb and effectively glue the wetted substrate at ∼10 kPa owing to the chaotropicity of Gua^+ moieties (Figure S17).

We then examined the underwater resistance of the adhesion. Two beef ribbons glued with the G-CSW suspension (2 wt %, pH 7) withstood a high shear rate underwater prior to failure (Movie S3). The underwater resistance of nanoparticle-mediated adhesion was further quantified as follows. Porcine skin assemblies glued with nanoparticles were immersed in phosphate buffered saline (PBS) at pH 7.4, and adhesion strengths were measured daily for 7 days (Figure 5b). The underwater adhesion of all bioorganic nanoparticles decreased with immersion time because water swells and detaches substrate polymer chains from the nanoparticle surface. In addition, increased hydration of surface functional groups weakens substrate−nanoparticle interactions. All chitin nanoparticles exhibited adhesion strengths >5 kPa after 1 week. G-CSW exhibited the greatest underwater adhesion strength (up to 10 kPa) because of the chaotropic nature of Gua^+. By contrast, the TM-50-mediated assembly did not endure 1 week underwater.

Strong underwater nanoparticle adsorption was further supported by adsorption test on gelatin hydrogels. Scanning electron microscopy (SEM) revealed that the gelatin hydrogel surface is densely covered by a matrix of adsorbed nanoparticles gelatin that was not removed by vigorous rinsing with water (Figure S18).

Hemostatic, Antibacterial, and Biocompatible Properties of the Nanoparticles

In addition to their adhesion properties, the nanoparticles should promote wound healing. Hence, we investigated their hemostatic and antibacterial abilities to prevent blood loss and protect wounds against bacterial infection.

During hemostasis, a platelet plug forms at the injured site, and coagulation factors transform fibrinogen into fibrin, which recruits blood cells to strengthen the plug (Figure 6a). T-CHW, Z-CHW, and G-CSW coagulated defibrinated blood within 10 min, suggesting that they mimic fibrin and form blood clots through noncovalent interactions enabled by their acetamide (−NHCO−) groups[51] (Figures S19 and S20). CNC, T-CHW, and G-CSW presented positive hemostatic properties with fibrinated blood. G-CSW was the most effective hemostatic agent, considering its shortest time for the clot to form (R), and reach a fixed (K), and maximum strength (TMA) and greatest fibrin accumulation rate (α) and clot strength (MA) (Figure 6b,c). This can be linked with the strong binding of chaotropic Gua^+ to fibrin and other negatively charged hemostatic factors. Because CNC only coagulated fibrinated blood, we propose that its OSO_3^- group adheres to fibrin but does not interact with other negatively charged components.[52]

The antibacterial properties of the bioorganic nanoparticles were examined using Gram-negative *Escherichia coli* and Gram-positive *Staphylococcus aureus*. The growth of both bacteria gradually decreased and was inhibited after exposure to G-CSW, suggesting a bactericidal effect. However, their growth was reduced but not inhibited when exposed to CSW (the nonadhesive precursor of G-CSW), indicative of a bacteriostatic mechanism (Figure 6d). The predominant antibacterial effect of G-CSW over CSW is attributed to the stronger binding of Gua^+ over NH_3^+ to negatively charged sites on the cytoplasmic membrane or cell wall of bacteria, which disrupts its permeability and induces intracellular-content leakage and cell lysis.[53] Furthermore, we observed that *S. aureus* was more sensitive to both G-CSW and CSW activities than *E. coli* (Figure S21) probably because the outer membrane of Gram-negative bacteria provides an additional protection against the nanoparticles.[54] CNC, T-CHW, and Z-CHW did not exhibit antibacterial properties (Figures S21 and S22) because the negatively charged groups on their surfaces can prevent nanoparticles from binding to bacteria.[28]

Possible inflammatory responses represent one of the biggest challenges associated with the use of crustacean-based materials.[55] To ensure biocompatibility, we examined whether G-CSW elicits an allergic immune response in mice administered with the ovalbumin (OVA) allergen, which is characterized by immunoglobulin E (IgE) reactions and immune cell infiltration in airways. While total and OVA-specific IgE levels in OVA/G-CSW mice were comparable to those in the PBS-treated group (blank control), they were higher in the OVA/alum-treated group (positive control) (Figure 6e). In addition, the levels of two types of immune cell, eosinophils and neutrophils, in G-CSW/OVA mice did not greatly increase compared with that of PBS mice and were 9- and 6-fold lower those of OVA/alum mice, respectively (Figure 6f). The total immune cell count in bronchoalveolar lavage fluid (BALF) of OVA/G-CSW mice was also comparable to that of regular mice (Figure S23). These results indicate that G-CSW is biocompatible *in vivo*.

Degradation Characteristic of the Nanoparticle Adhesive

A proper degradation rate of the bioorganic nanoparticle is crucial to maintain the adhesion during the wound healing period. Therefore, we investigated the *in vitro* degradation of G-CSW in PBS containing lysozyme, a ubiquitous enzyme in the human body that is capable of degrading chitin.[56,57] The weight of G-CSW gradually decreased with time, and ∼91 wt % remained after 1 week of incubation. As a control, CHW showed a faster degradation rate than G-CSW with 87 wt % remaining after 1 week (Figure 6g). The phenomenon can be attributed to the specificity of lysozyme, which can only recognize *N*-acetylglucosamine residues[57] but not guanidinium glucosamine residues present only in G-CSW. Another explanation can be the partial denaturation of lysozyme that resulted from the chaotropic effect of guanidinium cations.[20] In addition, the X-ray diffraction (XRD) pattern of G-CSW remained almost unchanged after enzymatic degradation (Figure 6h). The crystallinity index of G-CSW slightly increased from 93.15% (day 0) to 94.02% at (day 7) (Figure S24). These results suggest the preservation of the crystal

https://doi.org/10.1021/jacsau.1c00193
JACS Au 2021, 1, 1399−1411

structure (therefore cohesion strength) of the nanoparticle because lysozyme mainly hydrolyzes the more accessible amorphous region. Finally, the SEM image indicates that G-CSW maintained its needle-like morphology with unchanged dimensions after incubation in lysozyme (Figure 6i). Taken together, G-CSW is likely to show a proper biodegradation characteristic that can retain its underwater adhesion (at least 1 week) without causing significant allergic immune response in the body.

CONCLUSION

We showed that appropriately surface-modified chitin nanoparticles strongly bind together soft, wet hydrogels and biological tissue. Five types of chitin nanoparticles with various surface-charge densities were prepared as colloidally stable suspensions. Negatively charged, COO^--bearing particles glued gelatin hydrogels and porcine skin, whereas positively charged particles only exhibited adhesion when their surface NH_3^+ were converted into Gua^+. G-CSW were up to 3000-fold more adhesive than inorganic nanoparticles at the same concentration applied and maintained a ∼10 kPa strength underwater for 1 week. Compared with intensively studied mussel-inspired wet adhesives, G-CSW can glue at physiological pH without cytotoxic mediators. The glue does not require stringent storage conditions and is easy to spray on the substrate owing to is oxidation resistance and low viscosity.

Investigating the adhesion mechanism led to some principles for future applications and design of next-generation tissue adhesives. First, adhesion depends on the substrate surface, and the strength can be tuned by varying surface functional group contents of the nanoparticles, suggesting that the application can be tailored to a specific type of tissue. Second, adhesion involves strong cohesion strength inherent in highly crystalline chitin nanoparticles and particle−substrate interfacial multifaceted noncovalent interactions. The SFA study revealed that Gua^+ interacts 8.4-times more efficiently than primary NH_3^+ underwater. This feature relies on the chaotropic nature of Gua^+.

The biological benefits of chitin nanoparticles include rapid hemostasis, antimicrobial activity, *in vivo* biocompatibility, and a desired *in vitro* degradation characteristic which allows the maintenance of its crystal and adhesive features. Such multifunctional, high-performance materials combined with the simple yet robust nanobridging technique provide opportunities for multiple biomedical applications.

EXPERIMENTAL SECTION

Reagent information, nanoparticle synthesis and characterization, hydrogel preparation and characterization, and amino acid analyses of gelatin and porcine skin are detailed in the Supporting Information.

Adhesion of Nanoparticle Suspensions to Hydrogels and Biological Tissue

Hydrogels were cut into rectangular specimens (50 mm × 10 mm × 2.0 mm) with a thin-bladed scalpel. The thickness of the gel was fixed during preparation by adjusting the volume of the hydrogel precursor liquid according to the mold configuration. Porcine skin specimens with an average thickness of 1.524 mm were prepared similarly. No drying was performed on sample surfaces prior to testing. Bioorganic nanoparticle suspensions were tested at concentrations of 1, 2, and 3 wt % and pH 4 and 7. The aqueous TM-50 suspension was used as received (50 wt %, average pH 9).

A 30 μL aliquot of the nanoparticle suspension was evenly spread on one side of the substrate (the epidermis layer of the porcine skin) over 100 mm^2 area, that is, the overlapped region was 10 mm × 10 mm. The other substrate was then brought into contact and the whole assembly was pressed together for 1 min with a 1 kg calibration weight. The adhesion ability of the nanoparticle suspension was preliminarily confirmed by picking up and gently shaking the glued assembly. Suspension exhibiting adhesion abilities rendered the assembly intact. The glued assembly was equilibrated at 25 °C, 50% relative humidity (RH) for 2, 5, 15, 30, or 60 min (including 1 min pressing) prior to lap-shear test by tensile loading using a universal testing machine (Model 5943, Instron, U.K.) equipped with a 50 N load cell at a 10 mm min^{-1} speed at 25 °C according to the ASTM F2255-05 standard. The lap-shear rate and grip holding strength were maintained at constant values for all samples, and all experiments were conducted on the same day to minimize hydrogel aging. The adhesion strength was calculated using the equation $\tau_{ad} = F/A$, where τ_{ad} is the shear adhesion strength, F is the maximum force holding the glued assembly (failure force), and A is the glued area.

Underwater Adhesion

Porcine skin tissue was used as the substrate to avoid excess swelling-induced hydrogel fracture. To test the adhesion ability of nanoparticles to fully wetted surface, porcine skin was first immersed in deionized water for 15 min, and aqueous nanoparticle suspensions were then directly applied to the wetted skin without surface drying. Adhesion strength was measured after equilibrating the adhered wet assemblies for 2 or 60 min.

In another experiment, we tested the underwater resistance of nanoparticle adhesion to porcine skin. Skin tissue in its natural state was first glued with nanoparticle suspensions and equilibrated for 60 min. The glued skin-assembly junction was immersed in a 0.1 M PBS solution (pH 7.4) in a Petri dish, while the unglued part was rested on the dish edge. Adhesion strength was determined every 24 h for 1 week with the assembly removed and blotted dried with tissue prior to lap-shear testing.

Nanoparticle Adsorption on a Wet Surface

Underwater nanoparticle adsorption onto gelatin was visualized by SEM. Porcine skin was not used to avoid destruction by the vacuum introduced during freeze-drying and SEM. Nanoparticle suspensions at 2 wt % were first evenly spread onto the gelatin surface at 0.3 μL mm^{-2}. The hydrogel was left under ambient conditions for 2 h for nanoparticle adsorption and then vigorously rinsed with deionized water to remove any nonadsorbed materials before lyophilization at ≤−40 °C. Each freeze-dried gelatin surface was coated with a Pt layer using a Q150 T Plus turbomolecular pumped coater (Quorum Technologies Ltd., U.K.) operating at 15 mA for 90 s. The coated samples were observed using a field-emission SEM (MIRA 3, Tescan, Czech Republic) equipped with a 15 kV electron gun and a secondary detector.

Molecular Quantification of the Adhesion Energy of Guanidinium-Mediated Noncovalent Interactions by SFA

Atomically smooth mica surfaces were first cleaved from ruby muscovite (Grade 1, S&J Trading Inc., U.S.A.) into 1 cm × 1 cm pieces in a dust-free laminar-flow hood. Each cut piece was then coated with a 50 nm thick silver layer using an E-beam evaporator (KVE-C300160, Korea Vacuum Tech). The coated mica sheets were glued (silvered face down) onto cylindrical silica disks (radius of curvature R = 2 cm) using epoxy resin glue (EPON 1004F, Exxon Chemicals, U.S.A.), and the disks were then mounted in the SFA following the configuration shown in Figure 3e.[36]

N-Gua-chitosan, chitosan, and PGA were separately dissolved in 10 mM sodium acetate buffered solution (pH 4) at 1 mg mL^{-1}. Each solution was filtered through a poly(vinylidene fluoride) (PVDF) syringe filter (pore size: 0.45 μm; Millipore, U.S.A.). To prepare the PGA surface, the mica surface was first amine-functionalized with (3-aminopropyl)triethoxysilane (APTES) solution (0.1 wt %).[58] The solution was dropped onto the mica surface and left to stand for 10 min, and unreacted APTES was thoroughly removed by washing with excess deionized water. The filtered solution was dropped onto the mica surface (or the amine-functionalized surface for PGA) glued onto the SFA disk and left at room temperature for 1 h. Unreacted

https://doi.org/10.1021/jacsau.1c00193
JACS Au 2021, 1, 1399−1411

chemicals were thoroughly removed by washing with a sodium acetate buffer solution.

Intermolecular force−distance functions, $F(D)$, between two surfaces (i.e., chitosan vs gelatin, *N*-Gua-chitosan vs gelatin, chitosan vs PGA, and *N*-Gua-chitosan vs PGA) in 10 mM sodium acetate solution (pH 4) were determined using an SFA 2000 (Surforce LLC, U.S.A.). The surface-separation distance was monitored using interference fringes of equal chromatic order (FECO) generated from the silvered mirror layer by multiple beam interferometry (MBI). The mica−mica contact distance in air was used as the reference distance, that is, $D = 0$. The two coated mica surfaces were brought into molecular contact at the steric wall, D_{sw} (Figure 3e). After 10 min equilibrium, the surfaces were progressively separated until they abruptly separated. The distance at which the two surfaces suddenly separated was used to calculate the adhesion force (F_{ad}) using Hook's law. The Derjaguin approximation was used to relate the force between two spheres of equal radius R, normalized by the radius (F/R), separated at a small distance ($D \ll R$) in terms of energy per unit area (W) of two flat surfaces at the same D. Johnson−Kendall−Roberts (JKR) theory was used to calculate the adhesion energy per unit area ($W_{ad} = F_{ad}/1.5\pi R$) for soft and elastic surfaces.[36,50] SFA experiments were performed at four different positions ($n = 4$).

Blood Rheology

The hemostatic properties of the nanoparticles were investigated based on their ability to coagulate physically defibrinated sheep blood (Carolina Biological Supply Company, U.S.A.). The blood coagulation process was monitored using an MCR 302 modular compact rheometer (Anton Paar, Austria) at 25 °C. The blood was mixed with the nanoparticle suspension (2 wt %, pH 4) or double-deionized water (reference) in a 9:1 volume ratio in an ice bath. The blood mixture (200 μL) was then injected between parallel metal plates separated by 0.5 cm. A time sweep of 20 min at a 5% strain and a 5 rad s^{-1} frequency was conducted to identify the time required for blood clotting, after which a frequency sweep from 0.05 to 500 rad s^{-1} at a 5% strain was conducted to evaluate the stability of the blood clot. Rheological parameters, including the storage moduli G' and loss moduli G'' of sheep blood treated with different nanoparticles were recorded and plotted against time.

Thromboelastography

The *in situ* hemostatic dynamics of the nanomaterials were investigated through thromboelastographic measurement using a TEG Hemostasis Analyzer System 5000 (Hemonetics, U.S.A.). The 2 wt % suspension of each nanomaterial in DPBS was added to 320 μL of dog blood, which was provided in citrate-phosphate-dextrose solution with adenine (CPDA; anticoagulant and preservative solution, Korea Animal Blood Bank). Then, 20 μL of 200 mM aqueous $CaCl_2$ solution was added to the blood before loading into a disposable loading cup (REF 07-052, Hemonetics). Thromboelastographic parameters were collected under swirling of the torsional wire and pin which were immersed in blood samples.

Antibacterial Testing

The antibacterial properties of the nanoparticles were examined according to the ATSM-E2149 standard. Gram-negative, chemically competent DH5α *Escherichia coli* (enzynomics, South Korea) and Gram-positive *Staphylococcus aureus* sp. *aureus* (Microbiologics CCARM 0078, Thermo Fisher Scientific, U.S.A.) cells were streaked on lysogeny agar (10 g L^{-1} peptone, 5 g L^{-1} yeast extract, 10 g L^{-1} NaCl, 20 g L^{-1} agar, pH 7.4; Becton Dickinson, U.S.A.) and allowed to grow at 37 °C. A single bacterial colony was then inoculated into lysogeny broth (without agar), and the culture was grown in a shaking incubator (BioFree, South Korea) programmed at 37 °C, 180 rpm until the optical density at 600 nm (OD 600) was >1. In the well-diffusion assay, 100 μL of the bacterial suspension diluted to an OD 600 of 0.1 with double-deionized water (~8×10^7 CFU mL^{-1}) was spread on lysogeny agar plates using a Drigalski spatula until completely dry. A sterile cork borer was then used to make wells (~6 mm diameter) on the agar plate, and 30 μL of the as-prepared nanoparticle suspension (0.2 wt %) was pipetted into each well. No pH adjustment was done to the nanoparticle suspension to eliminate the effect of pH on bacterial growth. Double-deionized water was used as a negative control, while 0.1 M $CuSO_4$ solution was used as a positive control. The plates were incubated at 37 °C for 24 h and examined for inhibition zones around the wells.

The growth kinetics of *E. coli* and *S. aureus* suspensions in lysogeny broth supplemented with different nanoparticles were monitored. Bacterial suspensions were grown in a shaking incubator at a starting OD 600 of ~0.1, and aliquots were withdrawn every 2 h for 1 day for OD 600 reading. Nanoparticles were supplemented at 0.2 wt % (with respect to volume of culture medium) after incubation for 4 h as the bacteria entered the log phase, followed by vortexing and continued incubation. OD 600 values were measured using an UV−vis spectrometer (UV-2600, Shimadzu Corp., Kyoto, Japan).

The time-killing kinetics of antibacterial bioorganic nanoparticles were investigated using the plate count method. *E. coli* and *S. aureus* suspensions at OD600 of ~0.1 in lysogeny broth were incubated with the tested nanoparticles (0.2 wt %) in a shaking incubator. Aliquots of the bacterial cultures were withdrawn every hour for 12 h, appropriately diluted with double-deionized water, and evenly spread on lysogeny agar plates. The plates were then incubated at 37 °C to enumerate living cells after 24 h, expressed as CFU mL^{-1}.

In Vivo Allergic Immune Responses

Mice were intraperitoneally sensitized with 75 μg of OVA plus 100 mg of acetic acid, 2 mg of alum (Alhydrogel adjuvant 2%, vac-alu-250, InvivoGen), or 100 mg of G-CSW on day 0, and 7.50 μg of OVA was intranasally instilled to induce OVA-specific immune responses in the airway on days 14, 15, and 16. Mice intraperitoneally sensitized with PBS on day 0 (without further OVA challenge) were used as blank controls. The mice were euthanized 4 h after the last challenge. BALF and serum samples were collected for further analysis. BALF cells were manually counted using a hemocytometer and further analyzed by flow cytometry. Eosinophils and neutrophils were characterized by $CD11b^{int}$ sigle cF^{+} and $CD11b^{+}Gr\text{-}1^{+}$ cells, respectively. Serum and OVA-specific IgE levels were measured using a mouse IgE ELISA quantification set (Bethyl Laboratories, U.S.A.). All *in vivo* procedures were approved by the Pohang University of Science and Technology Institutional Animal Care and Use Committee prior to animal experimentation (IRB number: POSTECH-2019−0014).

In Vitro Degradation

PBS (0.1 M, pH 7.4) was first sterilized by filtering through a 0.22 μm-pore filter membrane. Chitin-based nanoparticles (250 mg) were dried in a vacuum oven at 60 °C to remove absorbed moisture until a constant weight was obtained (m_0). The dried nanoparticles were immediately dispersed into the PBS filtrate (10 mL) in a conical tube to which lysozyme extracted from chicken egg white (Sigma-Aldrich, U.S.A.) was added (0.5 mg mL^{-1}), and the mixture was vortexed thoroughly. Although nanoparticles were not colloidally stable in the high-ionic-strength buffer, it was assumed that particle aggregation did not significantly affect the enzyme activity or the degradation behavior of the nanoparticles. The mixture was then incubated in a shaking incubator (37 °C, 180 rpm). At investigation time points, the tubes were taken out and centrifuged at 8000 rpm for 10 min. The nanoparticle pellets were recovered, rinsed with deionized water to remove the enzyme and dissolved reducing sugar hydrolysates, and centrifuged again using the same setting. The pellets were then vacuum-dried at 60 °C until a constant weight (m_1). To prevent erroneous weight loss, the pellets were weighed together with the conical tubes, the weight of which was predetermined before the experiment. The nanoparticle mass remained after enzymatic hydrolysis was determined by taking the ratio of m_1 to m_0 and expressed in percentage. In addition, the crystal structure and morphology of nanoparticles after 7 day enzymatic degradation were studied using XRD and SEM, respectively (detailed configurations in the Supporting Information).

https://doi.org/10.1021/jacsau.1c00193
JACS Au 2021, 1, 1399−1411

■ ASSOCIATED CONTENT

Supporting Information

The Supporting Information is available free of charge at https://pubs.acs.org/doi/10.1021/jacsau.1c00193.

Reagent information, additional experimental details, and additional supporting results and discussion; Schemes S1 and S2, Figures S1−S24, and Tables S1−S6 (PDF)

Comparing the adhesion to gelatin hydrogel (23 wt %) between a commercial LUDOX TM-50 colloidal silica suspension (50 wt %, pH ∼ 9) and a laboratory-synthesized G-CSW suspension (2 wt %, pH 4) (MP4)

Sprayability of the G-CSW suspension (2 wt %, pH 7) to adhere gelatin hydrogels (MP4)

Underwater adhesion to beef connective tissue at high shear stress of the G-CSW suspension (2 wt %, pH 7) (MP4)

■ AUTHOR INFORMATION

Corresponding Authors

Sung Yeon Hwang − *Research Center for Bio-based Chemistry, Korea Research Institute of Chemical Technology (KRICT), Ulsan 44429, Republic of Korea; Advanced Materials and Chemical Engineering, University of Science and Technology (UST), Daejeon 34113, Republic of Korea;* orcid.org/0000-0002-4618-2132; Email: crew75@krict.re.kr

Dong Soo Hwang − *Division of Environmental Science and Engineering, Pohang University of Science and Technology (POSTECH), Pohang 37673, Republic of Korea;* orcid.org/0000-0002-2487-2255; Email: dshwang@postech.ac.kr

Jeyoung Park − *Research Center for Bio-based Chemistry, Korea Research Institute of Chemical Technology (KRICT), Ulsan 44429, Republic of Korea; Advanced Materials and Chemical Engineering, University of Science and Technology (UST), Daejeon 34113, Republic of Korea;* orcid.org/0000-0002-9369-1597; Email: jypark@krict.re.kr

Dongyeop X. Oh − *Research Center for Bio-based Chemistry, Korea Research Institute of Chemical Technology (KRICT), Ulsan 44429, Republic of Korea; Advanced Materials and Chemical Engineering, University of Science and Technology (UST), Daejeon 34113, Republic of Korea;* orcid.org/0000-0003-3665-405X; Email: dongyeop@krict.re.kr

Authors

Lam Tan Hao − *Research Center for Bio-based Chemistry, Korea Research Institute of Chemical Technology (KRICT), Ulsan 44429, Republic of Korea; Advanced Materials and Chemical Engineering, University of Science and Technology (UST), Daejeon 34113, Republic of Korea;* orcid.org/0000-0001-9791-6071

Sohee Park − *Division of Environmental Science and Engineering, Pohang University of Science and Technology (POSTECH), Pohang 37673, Republic of Korea*

Seunghwan Choy − *Biomedical Institute for Convergence, Sungkyunkwan University, Suwon 16419, Republic of Korea*

Young-Min Kim − *Division of Integrative Biosciences and Biotechnology, Pohang University of Science and Technology (POSTECH), Pohang 37673, Republic of Korea*

Seung-Woo Lee − *Division of Integrative Biosciences and Biotechnology and Department of Life Sciences, Pohang University of Science and Technology (POSTECH), Pohang 37673, Republic of Korea*

Yong Sik Ok − *Korea Biochar Research Center, APRU Sustainable Waste Management Program, Division of Environmental Science and Ecological Engineering, Korea University, Seoul 02841, Republic of Korea;* orcid.org/0000-0003-3401-0912

Jun Mo Koo − *Research Center for Bio-based Chemistry, Korea Research Institute of Chemical Technology (KRICT), Ulsan 44429, Republic of Korea*

Complete contact information is available at: https://pubs.acs.org/10.1021/jacsau.1c00193

Author Contributions

○These authors contributed equally: L.T.H., S.P., and S.C.

Author Contributions

L.T.H., S.P., and S.C. performed the experiments and analyzed the data. L.T.H., J.P., and D.X.O. prepared the figures and wrote the manuscript. S.Y.H., D.S.H., J.P., and D.X.O. conceived, designed, and directed the project. J.M.K. chemically modified chitin. Y.S.O. filed reference literatures and validated the manuscript. Y.-M.K. and S.-W.L. performed the *in vivo* experiments. All authors approved the final version of the manuscript.

Notes

The authors declare no competing financial interest.

■ ACKNOWLEDGMENTS

This work was supported by the Korea Research Institute of Chemical Technology (KRICT) (SS2142-10), the Bio-Industrial Technology Development Program (20008628) funded by the Ministry of Trade, Industry & Energy (MI, Korea), and the Basic Science Research Program through the National Research Foundation of Korea (NRF) and funded by the Ministry of Science, ICT, and Future Planning (2019R1C1C1003888).

■ REFERENCES

(1) Oh, D. X.; Kim, S.; Lee, D.; Hwang, D. S. Tunicate-mimetic nanofibrous hydrogel adhesive with improved wet adhesion. *Acta Biomater.* **2015**, *20*, 104−112.

(2) Taboada, G. M.; Yang, K.; Pereira, M. J. N.; Liu, S. S.; Hu, Y.; Karp, J. M.; Artzi, N.; Lee, Y. Overcoming the translational barriers of tissue adhesives. *Nat. Rev. Mater.* **2020**, *5* (4), 310−329.

(3) Nam, S.; Mooney, D. Polymeric Tissue Adhesives. *Chem. Rev.* **2021**, DOI: 10.1021/acs.chemrev.0c00798.

(4) Li, J.; Celiz, A. D.; Yang, J.; Yang, Q.; Wamala, I.; Whyte, W.; Seo, B. R.; Vasilyev, N. V.; Vlassak, J. J.; Suo, Z.; Mooney, D. J. Rough adhesives for diverse wet surfaces. *Science* **2017**, *357* (6349), 378−381.

(5) Ryu, J. H.; Messersmith, P. B.; Lee, H. Polydopamine surface chemistry: a decade of discovery. *ACS Appl. Mater. Interfaces* **2018**, *10* (9), 7523−7540.

(6) Zhang, C.; Wu, B.; Zhou, Y.; Zhou, F.; Liu, W.; Wang, Z. Mussel-inspired hydrogels: from design principles to promising applications. *Chem. Soc. Rev.* **2020**, *49* (11), 3605−3637.

(7) Rose, S.; Prevoteau, A.; Elzière, P.; Hourdet, D.; Marcellan, A.; Leibler, L. Nanoparticle solutions as adhesives for gels and biological tissues. *Nature* **2014**, *505* (7483), 382−385.

(8) Kim, J.-H.; Kim, H.; Choi, Y.; Lee, D. S.; Kim, J.; Yi, G.-R. Colloidal mesoporous silica nanoparticles as strong adhesives for

hydrogels and biological tissues. *ACS Appl. Mater. Interfaces* **2017**, *9* (37), 31469−31477.
(9) Shin, K.; Choi, J. W.; Ko, G.; Baik, S.; Kim, D.; Park, O. K.; Lee, K.; Cho, H. R.; Han, S. I.; Lee, S. H.; Lee, D. J.; Lee, N.; Kim, H.-C.; Hyeon, T. Multifunctional nanoparticles as a tissue adhesive and an injectable marker for image-guided procedures. *Nat. Commun.* **2017**, *8* (1), 15807.
(10) Wu, H.; Li, F.; Wang, S.; Lu, J.; Li, J.; Du, Y.; Sun, X.; Chen, X.; Gao, J.; Ling, D. Ceria nanocrystals decorated mesoporous silica nanoparticle based ROS-scavenging tissue adhesive for highly efficient regenerative wound healing. *Biomaterials* **2018**, *151*, 66−77.
(11) Meddahi-Pellé, A.; Legrand, A.; Marcellan, A.; Louedec, L.; Letourneur, D.; Leibler, L. Organ repair, hemostasis, and *in vivo* bonding of medical devices by aqueous solutions of nanoparticles. *Angew. Chem., Int. Ed.* **2014**, *53* (25), 6369−6373.
(12) Gao, Y.; Han, Y.; Cui, M.; Tey, H. L.; Wang, L.; Xu, C. ZnO Nanoparticles as an antimicrobial tissue adhesive for skin wound closure. *J. Mater. Chem. B* **2017**, *5* (23), 4535−4541.
(13) Matter, M. T.; Starsich, F.; Galli, M.; Hilber, M.; Schlegel, A. A.; Bertazzo, S.; Pratsinis, S. E.; Herrmann, I. K. Developing a tissue glue by engineering the adhesive and hemostatic properties of metal oxide nanoparticles. *Nanoscale* **2017**, *9* (24), 8418−8426.
(14) Okada, M.; Nakai, A.; Hara, E. S.; Taguchi, T.; Nakano, T.; Matsumoto, T. Biocompatible nanostructured solid adhesives for biological soft tissues. *Acta Biomater.* **2017**, *57*, 404−413.
(15) Tardy, B. L.; Richardson, J. J.; Greca, L. G.; Guo, J.; Ejima, H.; Rojas, O. J. Exploiting supramolecular interactions from polymeric colloids for strong anisotropic adhesion between solid surfaces. *Adv. Mater.* **2020**, *32* (14), 1906886.
(16) Soenen, S. J.; Parak, W. J.; Rejman, J.; Manshian, B. (Intra)Cellular stability of inorganic nanoparticles: effects on cytotoxicity, particle functionality, and biomedical applications. *Chem. Rev.* **2015**, *115* (5), 2109−2135.
(17) Sato, N.; Aoyama, Y.; Yamanaka, J.; Toyotama, A.; Okuzono, T. Particle adsorption on hydrogel surfaces in aqueous media due to van der Waals attraction. *Sci. Rep.* **2017**, *7* (1), 6099.
(18) Mogaki, R.; Hashim, P. K.; Okuro, K.; Aida, T. Guanidinium-based "molecular glues" for modulation of biomolecular functions. *Chem. Soc. Rev.* **2017**, *46* (21), 6480−6491.
(19) Heyda, J.; Okur, H. I.; Hladílková, J.; Rembert, K. B.; Hunn, W.; Yang, T.; Dzubiella, J.; Jungwirth, P.; Cremer, P. S. Guanidinium can both cause and prevent the hydrophobic collapse of biomacromolecules. *J. Am. Chem. Soc.* **2017**, *139* (2), 863−870.
(20) Mason, P. E.; Neilson, G. W.; Dempsey, C. E.; Barnes, A. C.; Cruickshank, J. M. The hydration structure of guanidinium and thiocyanate ions: implications for protein stability in aqueous solution. *Proc. Natl. Acad. Sci. U. S. A.* **2003**, *100* (8), 4557−4561.
(21) Xu, B.; Jacobs, M. I.; Kostko, O.; Ahmed, M. Guanidinium group remains protonated in a strongly basic arginine solution. *ChemPhysChem* **2017**, *18* (12), 1503−1506.
(22) Jayakumar, R.; Menon, D.; Manzoor, K.; Nair, S. V.; Tamura, H. Biomedical applications of chitin and chitosan based nanomaterials—a short review. *Carbohydr. Polym.* **2010**, *82* (2), 227−232.
(23) Azuma, K.; Nishihara, M.; Shimizu, H.; Itoh, Y.; Takashima, O.; Osaki, T.; Itoh, N.; Imagawa, T.; Murahata, Y.; Tsuka, T.; Izawa, H.; Ifuku, S.; Minami, S.; Saimoto, H.; Okamoto, Y.; Morimoto, M. Biological adhesive based on carboxymethyl chitin derivatives and chitin nanofibers. *Biomaterials* **2015**, *42*, 20−29.
(24) Pang, J.; Bi, S.; Kong, T.; Luo, X.; Zhou, Z.; Qiu, K.; Huang, L.; Chen, X.; Kong, M. Mechanically and functionally strengthened tissue adhesive of chitin whisker complexed chitosan/dextran derivatives based hydrogel. *Carbohydr. Polym.* **2020**, *237*, 116138.
(25) Xu, Y.; Liang, K.; Ullah, W.; Ji, Y.; Ma, J. Chitin nanocrystal enhanced wet adhesion performance of mussel-inspired citrate-based soft-tissue adhesive. *Carbohydr. Polym.* **2018**, *190*, 324−330.
(26) Liu, H.; Feng, Y.; Cao, X.; Luo, B.; Liu, M. Chitin nanocrystals as an eco-friendly and strong anisotropic adhesive. *ACS Appl. Mater. Interfaces* **2021**, *13* (9), 11356−11368.
(27) Zhang, X.; Rolandi, M. Engineering strategies for chitin nanofibers. *J. Mater. Chem. B* **2017**, *5* (14), 2547−2559.
(28) Tran, T. H.; Nguyen, H. L.; Hwang, D. S.; Lee, J. Y.; Cha, H. G.; Koo, J. M.; Hwang, S. Y.; Park, J.; Oh, D. X. Five different chitin nanomaterials from identical source with different advantageous functions and performances. *Carbohydr. Polym.* **2019**, *205*, 392−400.
(29) Tsubokura, K.; Iwata, T.; Taichi, M.; Kurbangalieva, A.; Fukase, K.; Nakao, Y.; Tanaka, K. Direct guanylation of amino groups by cyanamide in water: catalytic generation and activation of unsubstituted carbodiimide by scandium(III) triflate. *Synlett* **2014**, *25* (09), 1302−1306.
(30) Reid, M. S.; Villalobos, M.; Cranston, E. D. Benchmarking cellulose nanocrystals: from the laboratory to industrial production. *Langmuir* **2017**, *33* (7), 1583−1598.
(31) Rahman, I. A.; Padavettan, V. Synthesis of silica nanoparticles by sol-gel: size-dependent properties, surface modification, and applications in silica-polymer nanocomposites—a review. *J. Nanomater.* **2012**, *2012*, 1−15.
(32) Kim, B. J.; Oh, D. X.; Kim, S.; Seo, J. H.; Hwang, D. S.; Masic, A.; Han, D. K.; Cha, H. J. Mussel-mimetic protein-based adhesive hydrogel. *Biomacromolecules* **2014**, *15* (5), 1579−1585.
(33) Lim, C.; Lee, D. W.; Israelachvili, J. N.; Jho, Y.; Hwang, D. S. Contact time- and pH-dependent adhesion and cohesion of low molecular weight chitosan coated surfaces. *Carbohydr. Polym.* **2015**, *117*, 887−894.
(34) Fukuzumi, H.; Saito, T.; Okita, Y.; Isogai, A. Thermal stabilization of TEMPO-oxidized cellulose. *Polym. Degrad. Stab.* **2010**, *95* (9), 1502−1508.
(35) Wang, H.; Qian, C.; Roman, M. Effects of pH and salt concentration on the formation and properties of chitosan−cellulose nanocrystal polyelectrolyte−macroion complexes. *Biomacromolecules* **2011**, *12* (10), 3708−3714.
(36) Lim, C.; Park, S.; Park, J.; Ko, J.; Lee, D. W.; Hwang, D. S. Probing nanomechanical interaction at the interface between biological membrane and potentially toxic chemical. *J. Hazard. Mater.* **2018**, *353*, 271−279.
(37) Kulcsár, Á.; Lavalle, P.; Voegel, J.-C.; Schaaf, P.; Kékicheff, P. Interactions between two polyelectrolyte multilayers investigated by the surface force apparatus. *Langmuir* **2004**, *20* (2), 282−286.
(38) Lim, C.; Huang, J.; Kim, S.; Lee, H.; Zeng, H.; Hwang, D. S. Nanomechanics of poly(catecholamine) coatings in aqueous solutions. *Angew. Chem., Int. Ed.* **2016**, *55* (10), 3342−3346.
(39) Anderson, T. H.; Yu, J.; Estrada, A.; Hammer, M. U.; Waite, J. H.; Israelachvili, J. N. The Contribution of DOPA to substrate-peptide adhesion and internal cohesion of mussel-inspired synthetic peptide films. *Adv. Funct. Mater.* **2010**, *20* (23), 4196−4205.
(40) Yu, J.; Kan, Y.; Rapp, M.; Danner, E.; Wei, W.; Das, S.; Miller, D. R.; Chen, Y.; Waite, J. H.; Israelachvili, J. N. Adaptive hydrophobic and hydrophilic interactions of mussel foot proteins with organic thin films. *Proc. Natl. Acad. Sci. U. S. A.* **2013**, *110* (39), 15680−15685.
(41) Lin, Q.; Gourdon, D.; Sun, C.; Holten-Andersen, N.; Anderson, T. H.; Waite, J. H.; Israelachvili, J. N. Adhesion mechanisms of the mussel foot proteins mfp-1 and mfp-3. *Proc. Natl. Acad. Sci. U. S. A.* **2007**, *104* (10), 3782−3786.
(42) Yang, B.; Ayyadurai, N.; Yun, H.; Choi, Y. S.; Hwang, B. H.; Huang, J.; Lu, Q.; Zeng, H.; Cha, H. J. *In vivo* residue-specific DOPA-incorporated engineered mussel bioglue with enhanced adhesion and water resistance. *Angew. Chem., Int. Ed.* **2014**, *53* (49), 13360−13364.
(43) Kim, S.; Faghihnejad, A.; Lee, Y.; Jho, Y.; Zeng, H.; Hwang, D. S. Cation−π interaction in DOPA-deficient mussel adhesive protein mfp-1. *J. Mater. Chem. B* **2015**, *3* (5), 738−743.
(44) Lu, Q.; Hwang, D. S.; Liu, Y.; Zeng, H. Molecular interactions of mussel protective coating protein, mcfp-1, from *Mytilus californianus*. *Biomaterials* **2012**, *33* (6), 1903−1911.
(45) Lu, Q.; Danner, E.; Waite, J. H.; Israelachvili, J. N.; Zeng, H.; Hwang, D. S. Adhesion of mussel foot proteins to different substrate surfaces. *J. R. Soc., Interface* **2013**, *10* (79), 20120759.

https://doi.org/10.1021/jacsau.1c00193
JACS Au 2021, 1, 1399−1411

(46) Yu, J.; Wei, W.; Danner, E.; Israelachvili, J. N.; Waite, J. H. Effects of interfacial redox in mussel adhesive protein films on mica. *Adv. Mater.* **2011**, *23* (20), 2362−2366.
(47) Zhang, J.; Xiang, L.; Yan, B.; Zeng, H. Nanomechanics of anion-π interaction in aqueous solution. *J. Am. Chem. Soc.* **2020**, *142* (4), 1710−1714.
(48) Gebbie, M. A.; Wei, W.; Schrader, A. M.; Cristiani, T. R.; Dobbs, H. A.; Idso, M.; Chmelka, B. F.; Waite, J. H.; Israelachvili, J. N. Tuning underwater adhesion with cation−π interactions. *Nat. Chem.* **2017**, *9* (5), 473−479.
(49) Lu, Q.; Oh, D. X.; Lee, Y.; Jho, Y.; Hwang, D. S.; Zeng, H. Nanomechanics of cation-π interactions in aqueous solution. *Angew. Chem., Int. Ed.* **2013**, *52* (14), 3944−3948.
(50) Xiang, L.; Zhang, J.; Gong, L.; Han, L.; Zhang, C.; Yan, B.; Liu, J.; Zeng, H. Probing the interaction forces of phenol/amine deposition in wet adhesion: impact of phenol/amine mass ratio and surface properties. *Langmuir* **2019**, *35* (48), 15639−15650.
(51) Mommaerts, W. F. H. M. On the nature of forces operating in blood clotting. *J. Gen. Physiol.* **1945**, *29* (2), 103−112.
(52) Scarano, A.; Artese, L.; Piattelli, A.; Carinci, F.; Mancino, C.; Iezzi, G. Hemostasis control in endodontic surgery: a comparative study of calcium sulfate versus gauzes and versus ferric sulfate. *J. Endod.* **2012**, *38* (1), 20−23.
(53) Zhang, H.; Liu, Y.; Luo, T.; Zhao, Q.; Cui, K.; Huang, J.; Jiang, T.; Ma, Z. Synthesis of novel guanidine-based ABA triblock copolymers and their antimicrobial honeycomb films. *Polym. Chem.* **2018**, *9* (28), 3922−3930.
(54) Coma, V.; Deschamps, A.; Martial-Gros, A. Bioactive packaging materials from edible chitosan polymer—antimicrobial activity assessment on dairy-related contaminants. *J. Food Sci.* **2003**, *68* (9), 2788−2792.
(55) Van Dyken, S. J.; Mohapatra, A.; Nussbaum, J. C.; Molofsky, A. B.; Thornton, E. E.; Ziegler, S. F.; McKenzie, A. N. J.; Krummel, M. F.; Liang, H.-E.; Locksley, R. M. Chitin activates parallel immune modules that direct distinct inflammatory responses via innate lymphoid type 2 and $\gamma\delta$ T cells. *Immunity* **2014**, *40* (3), 414−424.
(56) Tomihata, K.; Ikada, Y. *In vitro* and *in vivo* degradation of films of chitin and its deacetylated derivatives. *Biomaterials* **1997**, *18* (7), 567−575.
(57) Liu, W.; Ma, Y.; Ai, L.; Li, W.; Li, W.; Li, H.; Zhou, C.; Luo, B. Enzymatic degradation of nanosized chitin whiskers with different degrees of deacetylation. *ACS Biomater. Sci. Eng.* **2019**, *5* (10), 5316−5326.
(58) Liu, Z.; Li, Z.; Zhou, H.; Wei, G.; Song, Y.; Wang, L. Immobilization and condensation of DNA with 3-aminopropyltriethoxysilane studied by atomic force microscopy. *J. Microsc.* **2005**, *218* (3), 233−239.

https://doi.org/10.1021/jacsau.1c00193
JACS Au 2021, 1, 1399−1411